

RSC Advances



This is an *Accepted Manuscript*, which has been through the Royal Society of Chemistry peer review process and has been accepted for publication.

Accepted Manuscripts are published online shortly after acceptance, before technical editing, formatting and proof reading. Using this free service, authors can make their results available to the community, in citable form, before we publish the edited article. This *Accepted Manuscript* will be replaced by the edited, formatted and paginated article as soon as this is available.

You can find more information about *Accepted Manuscripts* in the [Information for Authors](#).

Please note that technical editing may introduce minor changes to the text and/or graphics, which may alter content. The journal's standard [Terms & Conditions](#) and the [Ethical guidelines](#) still apply. In no event shall the Royal Society of Chemistry be held responsible for any errors or omissions in this *Accepted Manuscript* or any consequences arising from the use of any information it contains.

ARTICLE

Laser irradiated self-supporting and flexible 3-dimensional graphene-based film electrode with promising electrochemical properties

Cite this: DOI: 10.1039/

Qi Liu,^a Qiuwei Shi,^a Hongzhi Wang,^{*a} Qinghong Zhang^b and Yaogang Li^{*b}Received ooth
Accepted oothDOI: 10.1039/x0xx00000x
www.rsc.org/

Graphene, the last representative of sp² carbon materials, has been an ideal material platform for constructing flexible electronic devices. Exploring a new method to fabricate high-quality graphene films with more porous structure is a key for flexible electronic devices to achieve higher performance. The flexible solid-state supercapacitor based on 3-dimensional graphene film electrode is fabricated via filtration and laser irradiation method. The fabricated films with excellent mechanical properties display high electrical conductivity (8.53 Ω) and improved electrochemical performance (185 F/g). This 3-dimensional film is freestanding, which can thus be used directly as supercapacitor electrodes without external current collectors or binders that often used in commercial supercapacitors. Moreover, the films maintain excellent electrochemical properties under high stress and thus hold promise for being widely used in various energy storage devices.

Introduction

With the development of electronic products in the modern society, the flexibility is one of the development trends for future electronic devices. To meet aesthetic demands and the needs of specific environments, flexible electronic devices, such as wearable displays, rollable solar cells, artificial skin and stretchable sensors have caught great interest worldwide.¹⁻⁷ Obviously, these products need flexible energy storage devices. Supercapacitor, with simple structure, fast current response, high power density and reliable cycling stability and safety, has been one of the most promising solutions for this problem.⁸

Generally, supercapacitors can be divided into two categories according to the energy storage mechanism: electrical double layer capacitors (EDLCs) and pseudo-capacitors. Transition metal oxides, hydroxides⁹⁻¹⁰ and conducting polymers¹¹⁻¹² are usually used as the electrodes for pseudo-capacitors, in which fast and reversible faradic processes take place due to the electro-active species so that much higher pseudo-capacitance can be achieved.

However, pseudo-capacitors also have some drawbacks. The lack of cycling stability is due to the easy damaged structure of the materials during the redox reaction process, which limits the practical applications of such capacitors.¹³ Different from pseudo-capacitors, the capacitance of EDLCs stems from the pure electrostatic charge accumulation at the electrode/electrolyte interface, which is more reliable and safe. Carbon-based materials dominate the electrodes of this kind of capacitors because of their large surface area, high electrical conductivity and excellent mechanical strength, which perfectly compensates for the deficiencies of pseudo-capacitors.¹⁴

Graphene, among a large number of carbon-based materials, graphene, with a unique two-dimensional (2D) carbon nanostructure, has been an ideal material platform for constructing flexible EDLCs.¹⁵ This is because the graphene nanosheets can be easily fabricated into relatively large films, which has many excellent properties such as outstanding mechanical strength, superb chemical and thermal stability, excellent electrical conductivity and high surface-to-volume ratio.¹⁶⁻²⁰ In addition, recent literature reveals that graphene nanosheets can be easily fabricated in large quantities through chemical reaction from commercial graphite, which makes them more promising.²¹⁻²⁴ In most cases, however, a large portion of surface area of 2D graphene nanosheets becomes inaccessible because during the fabrication process, graphene nanosheets are vulnerable to irreversibly aggregate and restack as a result of van der Waals interaction.²⁵ Decreased surface area obstructs the

^aState Key Laboratory for Modification of Chemical Fibers and Polymer Materials, College of Materials Science and Engineering, Donghua University, Shanghai 201620, China. Email: wanghz@dhu.edu.cn;

^bEngineering Research Center of Advanced Glasses Manufacturing Technology, Donghua University, Shanghai 201620, China. Email: yaogang_li@dhu.edu.cn;

infiltration of electrolyte and the transportation of ions, lowering their energy density and limiting its commercial application.

Recently, the intrinsic capacitance of single-layer graphene has been reported to be $\sim 21 \text{ mF/cm}^2$, which is the ceiling of EDLCs and even of all carbon-based materials.²⁶ Thus, ECs based on graphene materials could, in principle, achieve an EDL capacitance as high as $\sim 550 \text{ F/g}$ if their entire surface area could be accessible. Graphene and its three-dimensional (3D) constructions have been widely used in various fields of research due to their outstanding characteristics.^{27–32} For the practical applications in these fields, scalable production of 3D porous graphene films is required, rather than 2D graphene sheets, because 3D porous films is better-performed on the electronic transmission, electrolyte penetration and the ion transport, which is the key to effectively solve the current problems of the supercapacitors.³³

In addition, the methods of synthesis of graphene films have been developed in recent years. These methods include vacuum filtering frozen solution³⁴, pressing graphene aerogel³⁵, and so on. Nonetheless, the 3D porous graphene films fabricated by these methods are lack of mechanical strength, and the electrochemical properties of these films are either not satisfying. In this paper, we attempt to prepare self-standing graphene films with 3D porous nanostructure by vacuum filtering and laser irradiation. Compact reduced graphene oxide films were used as the precursors which were fabricated through vacuum filtration and HI reduction. A series of 3D graphene films which have uniformly pores rapidly formed under laser irradiation. In this work, we demonstrated that the undesirable toxic iodide induced in graphene films by HI reduction can be readily removed through laser irradiation, and surprisingly, it was found that strong and superelastic graphene networks formed concurrently. Importantly, the light-assisted method allows us to alter the microstructure of macroscopic graphene materials, which was just meet the key to solve the problems of the supercapacitors as was mentioned above.

Experimental

1 Synthesis of graphite oxide by Hummers method³⁶

According to Hummer's method, graphene oxide (GO) was prepared using analytical grade reagents without further purification. Ultrapure Water ($18.2 \text{ M}\Omega$ resistance) was used in all experiments. Graphite (3.0 g) was added to cold ($0 \text{ }^\circ\text{C}$) concentrated H_2SO_4 (70 mL). Under vigorous agitation, KMnO_4 (9.0 g) was added to the solution slowly. After reaction at $35 \text{ }^\circ\text{C}$ for 2 h, 138 mL of water was added, and the solution was stirred for 15 min at $98 \text{ }^\circ\text{C}$. 420 mL H_2O_2 solution was then added to the mixture. Successively, the mixture was diluted by HCl aqueous solution with volume ratio of 1: 10 to remove metal ions. The resulting graphite oxide was isolated and washed by vacuum filtration for further use.

2 Preparation of 3D RGO films

In a typical experiment, 40 mL as-purified graphene oxide suspensions (2 mg/mL) were prepared and stirred for 15 min at room temperature.

Exfoliation of graphite oxide to GO was achieved by ultrasonication of the dispersion using a Branson Ultrasonic Cleaner (3510, 350 W) for 2 h and an ultrasonic probe (Ultrasonic products, FS-300, 300 W) for 15 min. The obtained brown dispersion was then subjected to 30 min of centrifugation at $3,000 \text{ r.p.m.}$ to remove any unexfoliated graphite oxide (usually present in a very small amount) using a centrifuge (Eppendorf 5702). Then the GO films were prepared by vacuum filtering the GO solution using a micro filtration membrane (pore diameter: $0.22 \mu\text{m}$), which were subsequently peeled off of the membrane and immersed into a 55% HI solution at room temperature for 1 h. The HI-reduced RGOs were washed with deionized water several times. The laser irradiated graphene films (L-RGO) were prepared using class IV laser product ($400\text{--}1100 \text{ nm CW}$; 1.25 W/cm^2). The fabricated RGO films were irradiated uniformly by the laser product for 120 s. The weight of the films was pre-estimated by the actual area of the films. The weight was then checked again after testing (after removing the electrolytes by dialysis and drying). If there was any inconsistency, the value obtained by direct weighing of the tested sample was used.

3 Characterization

The morphologies and the structure of the products were characterized by high-resolution field emission scanning electron microscopy (Hitachi S-4800). Raman spectroscopy measurements were performed on a Renishaw in plus laser micro-Raman system with excitation wavelength of 532 nm . The silicon peak at 520 cm^{-1} was used as a reference. The cyclic voltammetry (CV) and electrochemical impedance spectroscopy were measured using a three-probe method. Cylindrical hydrogel samples were sandwiched between two platinum foils and connected to a Zahner electrochemical workstation (Zen-nium) for cyclic voltammetry and electrochemical impedance spectroscopy. The mass specific capacitances were calculated from CV curves according to the equations $C_{\text{spec}} = 4C/M$ and $C/M = \int IdV/vmV$, where I is the current, v is the voltage scan rate, m is the total mass of both electrodes and V is the cell voltage.

Results and discussion

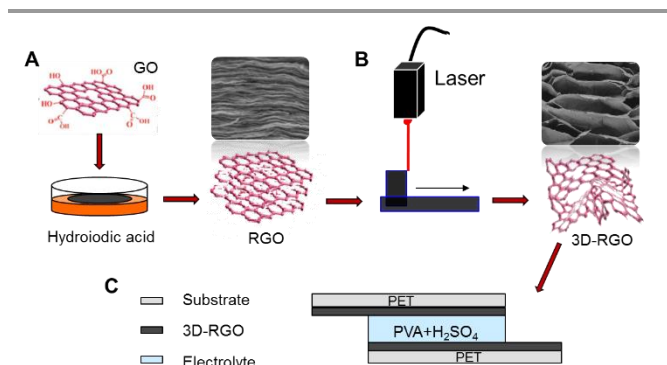


Fig. 1 Schematic illustration of the fabrication of laser-irradiated graphene-based supercapacitors. (A) A GO film is placed into the hydroiodic acid solution to be reduced. (B) As shown in the photograph, the RGO film changes from 2D compact structure to 3D porous structure after irradiated by laser. (C) Asymmetric supercapacitor is constructed from two identical L-RGO film electrodes, electrolyte, and PET substrate.

The typical schematic diagram of the fabrication process of free-standing laser irradiated graphene (L-RGO) films is shown in Fig. 1. The GO films were prepared by vacuum filtering the GO solution using a micro filtration membrane, which were subsequently peeled off from the membrane and immersed into a 55% HI solution at room temperature for 1 h. The HI-reduced RGOs were obtained (Fig. 1A). The L-RGO films were prepared by laser irradiating for 120 seconds (Fig. 1B), which has 3D porous microstructure. We finally assembled all-solid-state flexible supercapacitors using L-RGO films as an active electrode material. Fig. 1C shows the composition of the solid-state flexible supercapacitors. To assemble the solid-state supercapacitor, $\text{H}_2\text{SO}_4/\text{PVA}$ gel was used as the electrolyte.

1 Morphology analysis

Fig. 2a shows the cross-sectional field-emission scanning electron microscope (FESEM) images of the RGO films, from which it can be seen that the paper-like films have 2D compact structure. These samples are prepared by vacuum filtration of GO solution, followed by hydriodic acid (HI) reduction, washing and drying. As shown in Fig. 2b, c and d, the graphene films after laser irradiation have porous structure. The porous structure of the film is a result of the laser irradiation induced in the above process. After irradiating by laser, porous networks are formed and are permanent. The well-defined interconnected 3D porous network of the produced films is presented in Fig. 2b, c and d. Similar to the unirradiated graphene sample, the pores sizes of the network shown in the microstructure of the samples are in the range of submicrometer to several micrometers and the solid walls of these pores are composed of randomly cross-linked and intertwined graphene nanosheets.

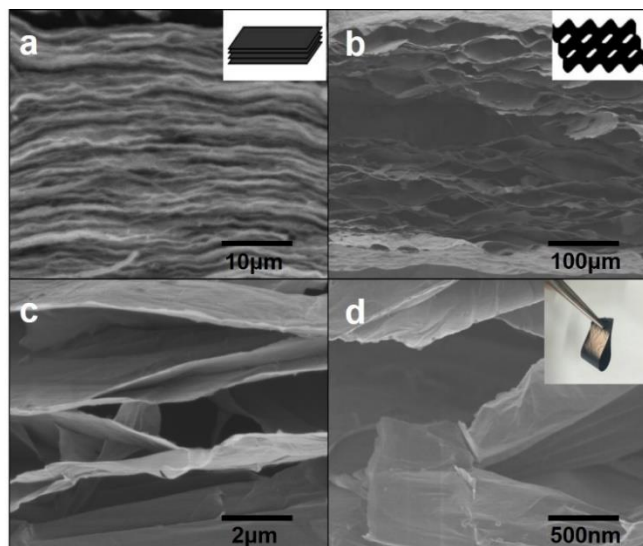


Fig. 2 FESEM images of 2D and 3D graphene films. (a) Low-magnification FESEM image of 2D graphene film. (b-d) Low-magnification and high-magnification FESEM image of 3D graphene film. (d) Inset is a photograph of the obtained 3D graphene film.

As the electrode material, the three-dimensional graphene skeleton network with various pores is beneficial for electrode to

fully contact with the electrolyte and can facilitate the transportation of electrons. Moreover, the specific surface area of the L-RGO films is improved. The contrast suggests that the L-RGO films can effectively prevent the restacking of graphene sheets and increase electrode material's surface area accessible to the electrolyte.

2 Raman and resistance analysis

The electronic structure change in the RGO and L-RGO sheets was further explored by Raman spectra (Fig. 3a). Analogously, after irradiation of laser, the intensity ratio of the D band (ca. 1340 cm^{-1}) to G band (ca. 1590 cm^{-1}), the D/G ratio, increased from 0.96 for the pure GO films to 1.45 for the L-RGO films, which is larger than 1.34 for the RGO films. The spectroscopic observations thus support the notion that more oxygenated groups in the graphitic planes are removed and the sp^2 planes are largely restored. The Raman spectrum reflects the reduced mechanism of GO to reduced graphene sheets in graphene-based films. These results manifest a trend of decrease in the average size of the sp^2 domains upon the reduction of GO.³⁷⁻³⁸ The voltage-current curve indicates that the resistance of L-RGO film ($8.53\ \Omega$) is much lower than RGO film ($17.36\ \Omega$). Additionally, the conductivity of these L-RGO ($8.1 \times 10^3\ \text{S/m}$) is even better than that of the RGO ($5.3 \times 10^3\ \text{S/m}$).

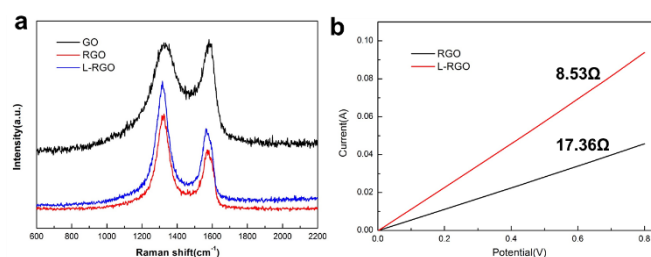


Fig. 3 (a) Raman spectra of GO, RGO and L-RGO. (b) Voltage-current curve of RGO and L-RGO.

3 Electrochemical properties analysis

To evaluate the performance of L-RGO films as electrochemical electrode, cyclic voltammetry (CV) measurements were performed, using a two-electrode cell in 1 M Na_2SO_4 solution. The scan-rate-dependent CVs of RGO and L-RGO film, with a range of scan rates of 5-100 mV/s and a potential window of 0-0.6 V, are illustrated by Fig. 4 shows the cyclic voltammograms (CV) of RGO films, L-RGO films in 1 M Na_2SO_4 aqueous solutions between 0 and 0.6 V at different scan rates. The CV curves of all these films show a typical shape, implying pure electric double layer capacitive behavior. L-RGO films show a larger current density in CV curves, implying a larger capacitance than RGO films. Even when the scan rate increases to 100 mV/s , the CV curve basically maintains the Faradaic peak-incorporated rectangle-like shape, similar to that observed at 5 mV/s , which is indicative of a quick charge-propagation capability of both the electric double layer capacitance. The specific capacitances (C_s) at different scan rates are calculated based on the CV measurements. The highest capacitance of 185 F/g have been achieved for the L-RGO films at scan rate of 5 mV/s , which are exceptionally higher than RGO

films (139 F/g) and GO films (103 F/g), especially the L-RGO films are free-standing and need no current collectors.

The reason that the L-RGO films possess a much higher capacitance than 2D compact RGO electrode probably owes to the unique porous networks films and the reduced graphene regions, which respectively leading to a dramatic increase in electrical conductivity along the vertical direction of the electrode. In order to evaluate the mechanical strength and cycling stability. CV cycling tests were performed at a scan rate of 100 mV/s for 200 bending cycles. As shown in Fig. 4c and e, the capacitance remains more than 90% of the initial capacitance, indicating the excellent mechanical stability of L-RGO film electrodes. To further quantify the capacitance of the L-RGO film electrode, a series of galvanostatic charge–discharge measurements were carried out at different current densities, and the typical charge–discharge curves are presented in Fig. 4f, which is in good agreement with their CV results.

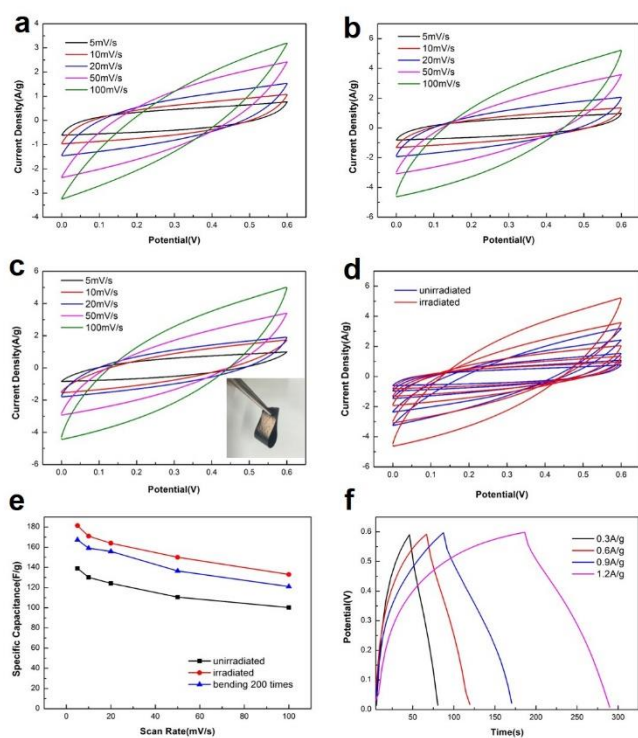


Fig. 4 (a) Cyclic voltammograms with different scan rates of RGO electrodes. (b) Cyclic voltammograms with different scan rates of L-RGO electrodes. (c) Cyclic voltammograms with different scan rates of L-RGO electrodes under repeated bending/extending tests. (d) Cyclic voltammograms contrast before and after laser irradiation. (e) Calculated specific capacitances from the CV curves at different scan rates of different samples. (f) Galvanostatic charge/discharge curves with different scan rates of L-RGO electrodes.

Further electrochemical investigation was carried out to determine the frequency response as well as the equivalent series resistance (ESR) of the symmetrical two-electrode measurement system based on fabricated materials. An electrochemical impedance spectroscopy (EIS) test was conducted at a frequency range of 0.1 Hz to 100 kHz for further evaluation of electrochemical behaviors of the RGO film electrodes and L-RGO film electrodes. The electrochemical impedance spectroscopy (EIS) plots of the RGO films and L-RGO films show in the Fig. 5. In the low frequency portion of the spectrum

of RGO films and L-RGO films, both impedance spectra tend towards a vertical line where the imaginary part of impedance rapidly increases, characteristic of capacitive behavior of the ion diffusion in the electrode structure. In the high frequency region a semicircle arc has been observed both in two lines and the charge transfer resistance can be directly compared through the semicircle diameter. It demonstrates that the electrode made of L-RGO has a charge transfer resistance lower than RGO, indicating the good conductivity of electrolyte and very low internal resistance of the electrode. In the low frequencies, the impedance plot turns into straight lines, and the shape of L-RGO films are more parallel to the imaginary axis than the shape of RGO, which indicates the attractive capacitive behavior of the device, representative of the ion diffusion in the electrode structure. The measured impedance spectra were analyzed based on an equivalent circuit, which is shown in the inset of Fig. 5. The calculated ohmic resistance R_t of L-RGO films were estimated to be quite low values of 8.9 Ω , in contrast to 19.7 Ω for RGO films, indicating the well-connected interfaces nature of electrode films, electrolyte ions, and current. In consideration of this, L-RGO films is a more ideal candidate for the electrode of supercapacitor.

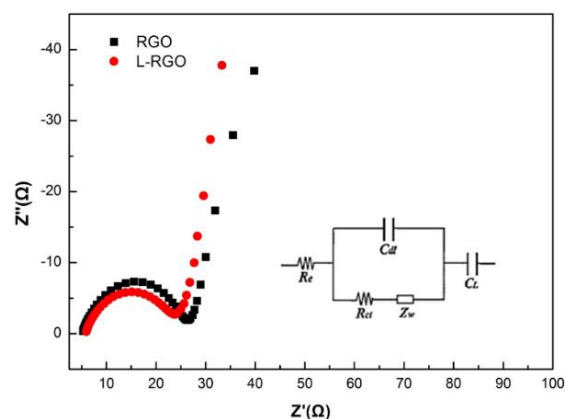


Fig. 5 Nyquistplots of graphene film electrode and laser irradiated graphene film electrode. Inset is a photograph of equivalent circuit.

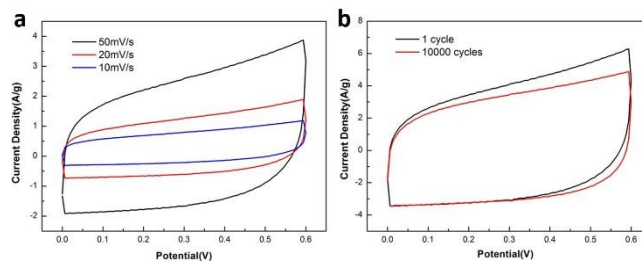


Fig. 6 Cyclic voltammograms of the supercapacitor based on L-RGO films, and the cycling stability of the all-solid-state supercapacitor after 10000 cycles with the scan rate of 50 mV/s.

In order to demonstrate the performance of the fabricated L-RGO electrodes for flexible energy storage, we finally assembled all-solid-state flexible supercapacitors using L-RGO films (1cm×4cm) as an active electrode material. Fig. 1c shows the composition of the solid-state flexible supercapacitors. To assemble the solid-state supercapacitor device, H_2SO_4/PVA gel was used as the electrolyte.

The thickness of the electrolyte was 1mm, and the ratio of H₂SO₄ and PVA was 1:1. The fabricated device was highly flexible and robust. The capacitive performance of the flexible solid-state supercapacitors was evaluated by CV (Fig. 6a) curves, which were obtained by testing the device under flat status. In general, the shape of the CV loop shows the Faradaic peak-incorporated rectangle-like shape, which indicates capacitance in the L-RGO electrode. The specific capacitances of the graphene hydrogel film electrode estimated from the CV curves were 150 F/g, substantially higher than those of most of the previously reported solid-state devices made of carbon nanotubes (50-115 F/g)³⁹⁻⁴⁰, and graphene films (62-120 F/g)⁴¹⁻⁴³. And what we need to emphasize is that: the electrode based on L-RGO itself is free-standing and without any current collector.

Conclusions

In summary, free-standing 3D porous graphene films were successfully prepared through laser irradiation. Then a symmetric supercapacitor was fabricated based on this film. An enhancement of capacitive behavior was shown on such device compared to supercapacitor based on 2D graphene film, owing to its unique 3D structure and the higher conductivity. This route of synthesis is rapid, easy and convenient. And the produced 3D porous graphene films would have promising applications in various flexible energy storage devices.

Acknowledgements

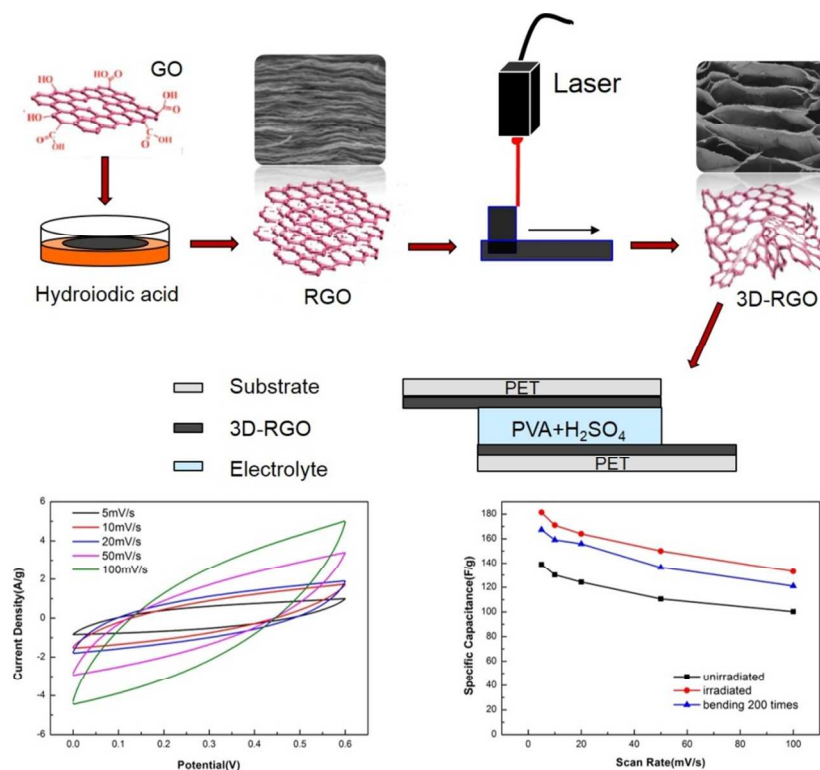
We gratefully acknowledge the financial support by NSF of China (No. 51172042), MOE of China (IRT1221, No.111-2-04), SRFDP (20110075130001), the Fundamental Research Funds for the Central Universities, and the financial support by the Graduate Innovation Fund of Donghua University (No. EG2015011)

References

- J. A. Rogers, T. Someya, Y. Huang, *Science*, 2010, 327, 1603.
- H. C. Ko, M. P. Stoykovich, J. Song, V. Malyarchuk, W. M. Choi, C. J. Yu, J. B. Geddes Iii, J. Xiao, S. Wang, Y. Huang, J. A. Rogers, *Nature*, 2008, 454, 748.
- H. Nishide, K. Oyaizu, *Science*, 2008, 319, 737.
- M. F. El-Kady, V. Strong, S. Dubin, R. B. Kaner, *Science*, 2012, 335, 1326.
- B. C. K. Tee, C. Wang, R. Allen, Z. Bao, *Nat. Nano.*, 2012, 7, 825.
- L. Peng, X. Peng, B. Liu, C. Wu, Y. Xie, G. Yu, *Nano Lett.*, 2013, 13, 2151.
- M. F. El-Kady, R. B. Kaner, *Nat. Commun.*, 2013, 4, 1475.
- P. Simon, Y. Gogotsi, *Nat. Mater.*, 2008, 7, 845.
- C. D. Lokhande, D. P. Dubal, O. S. Joo, *Curr. Appl. Phys.*, 2011, 11, 255.
- W. Deng, X. Ji, Q. Chen, C. E. Banks, *RSC Adv.*, 2011, 1, 1171.
- E. Frackowiak, V. Khomenko, K. Jurewicz, K. Lota, F. Beguin, *J. Power Sources*, 2006, 153, 413.
- G. A. Snook, P. Kao, A. S. Best, *J. Power Sources*, 2011, 196, 1.
- Y. Huang, J. Liang, Y. Chen, *Small*, 2012, 8, 1805.
- L. L. Zhang, X. S. Zhao, *Chem. Soc. Rev.*, 2009, 38, 2520.

- K. S. Novoselov, A. K. Geim, S. V. Morozov, D. Jiang, Y. Zhang, S. V. Dubonos, A. A. Firsov, *Science*, 2004, 306, 666.
- M. I. Katsnelson, *Mater. Today*, 2007, 10, 20.
- W. A. De Heer, C. Berger, X. Wu, P. N. First, E. H. Conrad, X. Li, G. Martinez, *Solid State Commun.*, 2007, 143, 92.
- L. Britnell, R. V. Gorbachev, R. Jalil, B. D. Belle, F. Schedin, M. I. Katsnelson, K. S. Novoselov, *Nano Lett.*, 2012, 12, 1707.
- D. A. Dikin, S. Stankovich, E. J. Zimney, R. D. Piner, G. H. B. Dommett, G. Evmenenko, S. T. Nguyen, R. S. Ruoff, *Nature*, 2007, 448, 457.
- A. A. Balandin, S. Ghosh, W. Z. Bao, I. Calizo, D. Teweldebrhan, F. Miao, C. N. Lau, *Nano Lett.*, 2008, 8, 902.
- S. Stankovich, D. A. Dikin, R. D. Piner, K. A. Kohlhaas, A. Kleinhammes, Y. Jia, Y. Wu, S. T. Nguyen, R. S. Ruoff, *Carbon*, 2007, 45, 1558.
- D. Li, M. B. Muller, S. Gilje, R. B. Kaner, G. G. Wallace, *Nat. Nanotechnol.*, 2008, 3, 101.
- S. Park, R. S. Ruoff, *Nat. Nanotechnol.*, 2009, 4, 217.
- S. Park, J. An, R. D. Piner, I. Jung, D. Yang, A. Velamakanni, S. T. Nguyen, R. S. Ruoff, *Chem. Mater.*, 2008, 20, 6592.
- Z. Q. Niu, J. Chen, H. H. Hung, J. Ma, X. D. Chen, *Adv. Mater.*, 2012, 24, 4144.
- J. Xia, F. Chen, J. Li, N. Tao, *Nat. Nanotechnol.*, 2009, 4, 505.
- C. Berger, Z. M. Song, X. B. Li, X. S. Wu, N. Brown, C. Naud, D. Mayou, T. B. Li, J. Hass, A. N. Marchenkov, E. H. Conrad, P. N. First and W. A. de Heer, *Science*, 2006, 312, 1191.
- F. Scarpa, S. Adhikari and A. S. Phani, *Nanotechnol.*, 2009, 20, 065709.
- Y. L. Shao, H. Z. Wang, Q. H. Zhang and Y. G. Li, *NPG Asia Mater.*, 2014, 6, e119.
- Y. X. Xu, K. X. Sheng, C. Li and G. Q. Shi, *ACS Nano*, 2010, 4, 4324.
- S. Han, D. Wu, S. Li, F. Zhang and X. Feng, *Adv. Mater.*, 2014, 26, 849-864.
- X. Cao, Y. Shi, W. Shi, G. Lu, X. Huang, Q. Yan, and H. Zhang, *Small*, 2011, 7, 3163-3168.
- X. Cao, Z. Yin, and H. Zhang, *Energy Environ. Sci.*, 2014, 7, 1850-1865.
- C. Y. Hou, H. Z. Wang, Q. H. Zhang, Y. G. Li, M. F. Zhu, *Adv. Mater.*, 2014, 26, 5018.
- F. Liu, S. Song, D. Xue, H. Zhang, *Adv. Mater.*, 2012, 24, 1089.
- W. S. Hummers, R. E. Offeman, *J. Am. Chem. Soc.*, 1958, 80, 1339.
- C. Y. Hou, H. Z. Wang, Q. H. Zhang, Y. G. Li, *J. Hazard. Mater.*, 2012, 205, 229.
- C. Y. Hou, H. Z. Wang, Q. H. Zhang, Y. G. Li, *Carbon*, 2012, 50, 1959.
- M. Kaempgen, C. K. Chan, J. Ma, Y. Cui, G. Gruner, *Nano Lett.*, 2009, 9, 1872.
- S. Hu, R. Rajamani, X. Yu, *Appl. Phys. Lett.*, 2012, 100, 104103.
- B. G. Choi, J. Hong, W. H. Hong, P. T. Hammond, H. Park, *ACS Nano*, 2011, 5, 7205.
- B. G. Choi, S. J. Chang, H. W. Kang, C. P. Park, H. J. Kim, W. H. Hong, S. Lee, Y. S. Huh, *Nanoscale*, 2012, 4, 4983.
- Z. Weng, Y. Su, D. W. Wang, F. Li, J. Du, H. M. Cheng, *Adv. Energy Mater.*, 2011, 1, 917.

Graphical Abstract



Rapid preparation of self-supporting and flexible 3-dimensional graphene-based film electrode with promising electrochemical properties by HI reduction and laser irradiation.